International Journal of Hydrogen Energy, Volume 102, February 2025, pp. 732-748
DOI:10.1016/j.ijhydene.2024.10.431

Enhanced Data-Driven Economic Assessment of Fuel Cell Electric Buses Utilising an Improved Markov Chain Monte Carlo Approach

Xinjie Yuan[1,a], Miao Xu[1,b], Zhongjun Hou[*, a], Wenchuang Chen[*,b],
Yun Huang[a], Jiaming Lv[a], Xudong Xu[a], Luofeng Huang[c]

a. Shanghai Hydrogen Propulsion Technology Co., Ltd., 1788 Xiechun Road, Shanghai, China, 201804

b. School of Civil Engineering, Sun Yat-Sen University, and Southern Marine Science and Engineering Guangdong Laboratory (Zhuhai), Zhuhai 519082, China

c. Faculty of Engineering and Applied Sciences, Cranfield University, Cranfield MK43 0AI, UK

* Corresponding author: Email: hou_zhongjun@shpt.com, chenwch37@mail.sysu.edu.cn

Abstract: Accurate economic assessment of proton exchange membrane fuel cell (PEMFC) vehicles is essential for optimizing control strategies in the PEMFC industry, which is largely driven by the need to reduce costs. Traditional data-driven approaches have focused on reconstructing typical driving cycles from real-world speed data, often overlooking the intensity and acceleration of these cycles. These factors are crucial for water and heat management in PEMFCs and can lead to inaccurate estimates of hydrogen consumption. This paper introduces a novel algorithm for typical driving cycles reconstruction based on real-world data, named the improved two-dimensional Markov Chain Monte Carlo (2D MCMC) approach using Metropolis-Hastings (M-H) sampling. The approach innovatively encodes the integration of real-time vehicle speed and acceleration sequences into a hierarchical 2D state transition probability matrix. To optimise both accuracy and computation time, the M-H based sampler is newly introduced to generate typical driving cycle without the computational burden of multiplying large matrices. Moreover, by integrating the agglomerative nesting

Published by Elsevier. This is the Author Accepted Manuscript issued with: Creative Commons Attribution License (CC:BY 4.0).
The final published version (version of record) is available online at DOI:10.1016/j.ijhydene.2024.10.431. Please refer to any applicable publisher terms of use.

(AGNES) alongside a comprehensive evaluation system that incorporates simulation and bench testing, the proposed approach effectively weights real-world route conditions in the economic assessment. Case studies involving 10 PEMFC hybrid buses in Shanghai, China, validate the effectiveness and robustness of the proposed method. Comparative analyses show that the relative errors in hydrogen consumption per 100 km between the reconstructed and real-world driving cycles are within 1.20-3.01% for all ten buses in Shanghai, with computation times reduced by up to 12.60% compared to the existing methods.

Keywords: Fuel cell electric bus (FCEB); Metropolis-Hastings (M-H); Markov Chain (MC); Driving cycle; Economic assessment.

1 Introduction

In recent years, hydrogen energy has emerged as a prominent clean and sustainable alternative to fossil fuels, particularly in the realm of fuel cell electric vehicles [1]. Among these, fuel cell electric buses (FCEBs) have garnered significant attention due to their potential for zero-emission transportation, coupled with extended operational ranges and rapid refuelling times [2]. This makes them a compelling solution for addressing the pressing challenges of green urban mobility. Therefore, the accurate assessment of the economic viability of FCEBs is paramount to the market penetration and development [3]. However, a pivotal challenge that undermines the precision of such evaluations lies in the disparity between real-world driving cycles and those simulated during testing phases. One of the key reasons for these inaccuracies is the imprecise description of driving conditions caused by the incongruence between actual test rigors and on-road performance dynamics. Compared to lithium-ion battery electric buses (BEBs) and internal combustion engine (ICE) buses, FCEBs exhibit a pronounced temperature lag issue that demands high accuracy in load transients [4]. Besides, the relatively limited sample size of FCEBs compared to BEBs and ICE buses necessitates more precise analyses of specific driving scenarios. Inaccurate representation of these scenarios can lead to misleading conclusions regarding the economic performance and durability of FCEBs.

Previous research in FCEBs real-time speed prediction could be classified into four primary types, random splicing of micro-trips, dimension reduction and clustering for driving cycle analysis, one-dimensional speed Markov Chain, and machine learning

[5]. The comparative results of these approaches are listed in Table 1. These conventional approaches hardly balance high weight of variable load in economic evaluation, small sample sizes of FCEBs, high demands for interpretability, convenient operation, and strong generalization ability.

Table 1: Comparative results of four primary methods for the design of driving cycles.

No.	Methods	Strengths	Limitations
1	Micro-trips random selection	• Easy operation • High interpretability	• Strong randomness • High computation costs • High requirement on data
2	Dimension reduction and clustering	• Easy operation • Low computation costs	• Low interpretability • Serious information losses • Uneven clustering distribution
3	Speed Markov Chain	• High interpretability • High robustness	• High computation costs • Low precision in load variations • Easily ensnared in localized transition
4	Machine learning	• High efficiency • Ability to predict complex patterns	• Low interpretability • High computational resources • High requirement on training datasets

First, The micro-trip approach outlined in Table 1, defined as short segments of vehicle driving cycles delimited by consecutive idling conditions, has been commonly employed in generating driving cycles [6]. However, its utility is constrained by the size and quality of the raw vehicle dataset. In [7], 803 valid micro-trips in Greater Cairo were selected from a pool of 10,942 and clustered using the K-means method to splice typical driving cycles. Comparisons with the American transient federal test procedure (FTP-75) cycle and the European modal cycle (ECE) revealed deviations in average cycle speed and average acceleration ranging from 9.339% to 29.488%, indicating significant volatility and instability heavily influenced by the scale and quality of raw data and micro-trips. In [8], two driving cycles were generated based on 1,087 and 4,333 micro-trips, respectively, for economic assessment. These cycles exhibited a 31%

difference in fuel consumption compared to FTP-75, primarily due to substantial disparities in speed and acceleration characteristics. While the micro-trip method offers ease of operation and high interpretability, its strong randomness, high data size and quality requirements, and substantial computational costs make it unsuitable for applications involving a limited number of proton exchange membrane fuel cell (PEMFC) vehicles.

Second, dimension reduction and clustering techniques have been designed to identify representative driving modes. In [9], unsupervised methods were employed, including principal components analysis (PCA) for dimension reduction and K-Means for clustering. These two approaches were applied together to explore the relationship between PEMFC system efficiency and driving styles using real-time vehicle data. A case study was conducted on a PEMFC logistics vehicle operating in Shanghai, based on a dataset of 312,641 entries. The 23 power-related features were transformed into 8 principal components. However, these new components, lacking specific physical interpretations, only represented 85% of the cumulative contribution, indicating significant information loss. Additionally, the uneven distribution of items in each cluster resulted in unrepresentative samples within each group. In [10], eight speed characteristics were selected for feature dimension reduction, followed by segment clustering. The techniques of dimension reduction and clustering are primarily applied to processing raw vehicle data, but the core operational method remains similarities to the concatenation of micro-trips. Therefore, while inheriting the inherent issues and limitations of micro-trip concatenation discussed above, this approach suffers from

problems such as notable information loss and issues of imbalanced clustering sample sizes. While effective in reducing data complexity, this approach may overlook crucial temporal dynamics and is heavily influenced by the number of clusters chosen.

Third, this approach involved utilizing a driving velocity Markov Chain to model speed sequences and generate driving cycles, rather than stitching together driving segments [11]. In [12], a conventional Markov Chain method was employed to establish the transition probability matrix (TPM) using velocity data. However, there was significant variation in acceleration/deceleration between the constructed driving cycle and real-world data, which required further refinement for accurate PEMFC system efficiency assessment. In [13], road slope was innovatively incorporated into the construction of the Markov Chain for heavy-duty vehicles (HDVs) for driving cycle generation. While Markov chains capture temporal dependencies, they often inadequately represent the joint distribution of speed and acceleration/deceleration, which is crucial for FCEBs due to their sensitivity to load transients. Furthermore, for FCEBs, the slope variations are much smaller than for HDVs. Route planning that considers bus stop stations and nearby refuelling stations should also be further considered.

Lastly, the fourth approach listed in Table 1 utilised neural networks to learn complex driving patterns. In [14], deep neural networks were employed to predict driving cycles, analyse the modelling strategy for electric vehicles, and estimate heat generation. However, the inaccuracy in forecasting velocity during WLTC, FTP75, and NEDC cycles varies significantly with the same amount of input data, indicating low

robustness of these methods across different routes and driving patterns. Additionally, due to their low interpretability, it was challenging and time-consuming to identify the reasons behind this low robustness. For FCEBs and other PEMFC vehicles with limited datasets, these methods, which heavily rely on the quantity and quality of training data, offer little explanatory power. Furthermore, considering the intricate electrochemical reactions of the PEMFC system, which were even harder to explain during real-world vehicle operation, the generated typical driving cycles should exhibit high interpretability relevant to the specific scenario. In [15], a learning vector quantization neural network (NN) was combined with PCA and K-means methods to identify driving patterns and predict electric vehicle velocity. The prediction accuracy was evaluated across four different prediction horizons to determine the most effective approach. However, the heavy reliance on a specific set of hyperparameters indicated potential limitations in robustness when applied to other datasets. While neural networks are powerful, they require large amounts of training data and may lack transparency in their decision-making process. Consequently, high-quality real-time vehicle datasets are crucial for training prediction models, which are currently limited for PEMFC vehicles due to their commercialization stage.

In summary, driving cycles are significant for vehicle performance evaluations including emissions and energy consumption estimations [16]. As summarised in Table 1, current methodologies predominantly focus on speed distribution in vehicle data analysis overlook crucial metrics such as acceleration/deceleration patterns [17]. However, the economic assessment and the efficiency of PEMFC systems are quite

sensitive to the rates of speed and power change different from electric vehicles. This oversight results in outcomes that approximate real-world vehicle speeds on an aggregate level but fail to accurately capture the temporal dynamics of vehicle behaviour. Consequently, these approaches may converge on local optima rather than accurately reflecting the nuanced temporal changes in vehicle dynamics over time.

The paper presents a novel approach to the economic assessment of PEMFC vehicles by introducing an improved two-dimensional Markov Chain Monte Carlo (2D MCMC) approach using Metropolis-Hastings (M-H). This work significantly contributes to the field through several innovative aspects:

1) **Introduction of Advanced Algorithms with improved Precision and Efficiency:** The incorporation of agglomerative nesting (AGNES) within the 2D MCMC framework using M-H sampling represents a novel hierarchical methodological advancement. The integration of real-time vehicle speed and acceleration enhances the accuracy of PEMFC vehicle economic assessments by addressing the variability in driving intensities and acceleration, which are often overlooked in traditional models. The proposed model demonstrates substantial improvements in both the precision of hydrogen consumption predictions and computational efficiency compared to existing models. The significant reduction in relative errors and computation time highlights the innovative and practical benefits of the approach.
2) **Comprehensive Evaluation System:** By coupling simulation with bench testing, the authors have created a robust evaluation system that better considers load

variations and their impact on PEMFC performance. This comprehensive approach is commendable and presents a novel pathway for achieving precise economic evaluations.

3) **Application to Real-World Cases:** The application of the novel algorithm to real-world data from ten PEMFC hybrid buses in Shanghai provides a practical demonstration of the approach's adaptability and success. This strengthens the manuscript's contribution by showing real-world applicability and effectiveness.

This paper is organised as follows. Section 2 presents the operation status of FCEBs in Shanghai, the novel application of the 2-D velocity-acceleration/deceleration MCMC algorithm and M-H sampling for the economic evaluation and driving cycle generation of FCEBs, key data for the case studies. In Section 3, the proposed algorithm is successfully verified and validated based on the simulation models and hardware-in-loop (HiL) bench test platform, using the real data from two FCEB routes. This section also includes three comparative analyses: comparisons with random slicing of driving cycles, one-dimensional Markov Chain, and two-dimensional Markov Chain with multiplication of matrices, to demonstrate the adaptability, accuracy, and low computational cost of the proposed method. The conclusions and future work are discussed in Section 4.

2 Fuel cell electric buses (FCEBs) and methodologies

2.1 Structure and routes of FCEBs

The studied Shenwo FCEB with the PEMFC system and the energy flow structure is presented in Appendix 1. The anode self-humidification PEMFC system as shown in

Appendix 1 (b) is independently developed by Shanghai Hydrogen Propulsion Technology Co. Ltd. The specifications of the $60\ kW$ PEMFC system with anode self-humidification installed on the studied bus are listed in Appendix 2 [18]. As shown in Appendix 1 (c), the vehicle control unit (VCU), as the core of the control system, is responsible for energy management to balance power requests and power outputs of PEMFC and battery [19]. Therefore, for a fixed energy management strategy in a PEMFC hybrid bus, the efficiency of the PEMFC system has a significant influence on hydrogen consumption under various driving styles.

As illustrated in Appendix 3, the Pujiang No. 10B (designated as Route 1) and Pujiang No. 13 (designated as Route 2) are key bus lines in Minhang District at 121.41°E, 31.07°N in Shanghai, China. In total, there are ten PEMFC buses operating on these routes in red and blue in Appendix 3, serving multiple key stations within the region. After completing the passenger-carrying tasks (working segment), both of these lines are unloaded to the Fengxian District Bus Parking and Maintenance Hydrogen Station for hydrogen refuelling (refuelling segment), ensuring continuous and efficient operation of the buses.

2.2 Proposed 2D MCMC algorithm

In this section, the application of the proposed hierarchical 2D MCMC algorithm using M-H sampling is explained in detail. An overview of the proposed method is described in Fig. 1. The procedure of the proposed method can be summarised into the four steps.

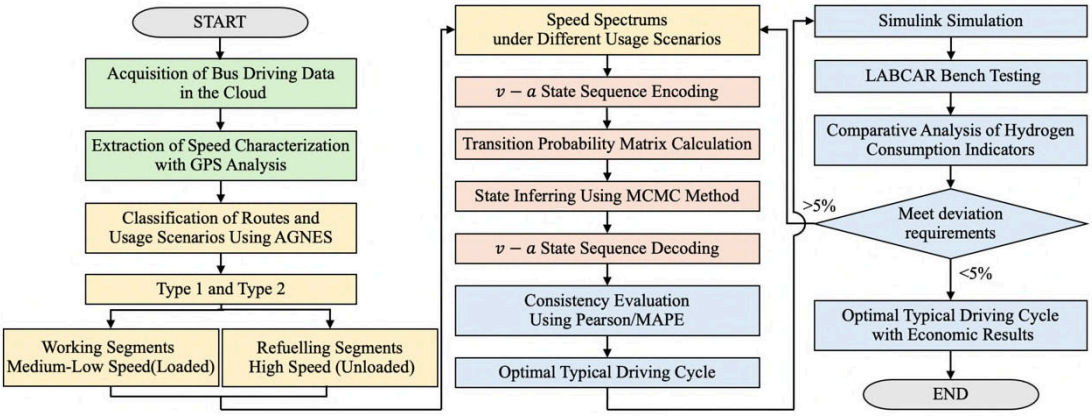


Fig. 1: Flow chart of the 2D MCMC algorithm.

Step 1 Acquisition of GPS data and extraction of speed characterization: In the realm of transportation and automotive industries, the collection of vehicle data plays a pivotal role in enhancing operational efficiencies, ensuring safety, and facilitating informed decision-making. The process of vehicle data collection routinely involves the integration of Global Positioning System (GPS) technology alongside a multitude of sensors and telemetry devices within vehicles [20]. Route segments can be identified based on sequences of GPS points and specific criteria such as proximity and order. The assessment criteria of the speed characteristics is referenced by the China Heavy-duty Commercial Vehicle Test Cycle for Bus (CHTC-B), a set of standardised driving conditions developed in China to test and assess the performance of urban buses under simulated real-world city driving conditions [21]. This protocol is generated from a series of predefined speed profiles derived from extensive empirical data. The definition of the speed characteristic in this study is benchmarked against the CHTC-B, which are widely adopted and recognized. The parameters are summarised in Table 2.

Table 2: Definition of the eleven characteristic assessment parameters benchmarked against the CHTC-B.

No.	Characteristics	Symbol	Unit	Definition
1	Maximum speed	v_{max}	km/h	The maximum value in the speed data
2	Maximum acceleration	a_{max}	m/s^2	The maximum acceleration in the speed data
3	Minimum deceleration	d_{max}	m/s^2	The maximum deceleration in the speed data
4	Average speed	v_{ave}	km/h	Average speed of entire speed data
5	Average running speed	v_{ars}	km/h	Average speed of entire running speed data
6	Average acceleration (>0)	a	m/s^2	Average acceleration of acceleration phases
7	Average deceleration (<0)	a	m/s^2	Average deceleration of deceleration phases
8	Ratio of acceleration	P_{acc}	%	Percentage of time spent in acceleration mode
9	Ratio of deceleration	P_{dec}	%	Percentage of time spent in deceleration mode
10	Ratio of cruising	P_{steay}	%	Percentage of time spent in cruising mode
11	Ratio of idling	P_{idle}	%	Percentage of time spent in idling mode

Step 2 Hierarchical clustering by integrating velocity and GPS signals: Agglomerative Nesting (AGNES) is a hierarchical clustering algorithm used to group samples in a dataset into clusters based on their similarity [22]. It begins by treating each sample as its own cluster and iteratively merges the most similar clusters until all samples belong to a single cluster. AGNES is advantageous for generating a complete hierarchical structure of clusters without needing prior knowledge of the number of clusters, which is adopted to realize the classification of types in this study. As a specific application of the AGNES, the Ward method is applied for hierarchical clustering, where the merging of clusters is based on minimizing the increase in the within-cluster sum of squares (WSS), as provided in Eqs. (1-3) [23]. The within-cluster sum of squares refers to the sum of squared distances from all points in a cluster to the centroid of that cluster. At each merge, the Ward method selects the two clusters whose merger results in the smallest increase in the within-cluster sum of squares.

$$\Delta WSS(C_{ij}) = \sum_{x \in C_i} \|x - \mu_{ij}\|^2 + \sum_{x \in C_j} \|x - \mu_{ij}\|^2 - (WSS(C_i) + WSS(C_j)) \quad (1)$$

$$\mu_i = \frac{1}{n_i}\sum_{x\in C_i} x\,;\quad \mu_{ij} = \frac{n_i\cdot\mu_i + n_j\cdot\mu_j}{n_i+n_j} \tag{2}$$

$$WSS(C_i) = \sum_{x\in C_i}\|x-\mu_i\|^2 \tag{3}$$

where C_i and C_j are different clusters; C_{ij} represents the cluster after merging; x represents a sample point in a cluster; μ_i, μ_j and μ_{ij} represent the centroid of clusters C_i, C_j and C_{ij} respectively; n_i and n_j respectively represent the count of elements in clusters C_i and C_j; $\|x-\mu_i\|^2$ represents the square of the Euclidean distance between sample point x and centroid μ_i.

Step 3 Advanced 2D hierarchical Metropolis-Hastings based Markov Chain: Integrating the obtained vehicle speed-time series data and characteristic evaluation parameters with GPS analysis results, followed by employing the AGNES method, enables the segmentation of bus operation into several distinct types and usage scenarios. Subsequently, specific to each type and each usage scenario, advanced hierarchical Markov chains are employed to generate representative driving cycles for buses. This process comprises four main steps:

a) v-a state sequence encoding: The original speed and acceleration/deceleration sequences are encoded from the original speed sequence into a discrete velocity-acceleration/deceleration state sequence $S_t = (v_t, a_t)$, where the acceleration/deceleration a_t at time t is defined in Eq. (4).

$$a_t = \frac{v_{t+1}-v_t}{t_{t+1}-t_t} \tag{4}$$

where v_{t+1} and v_t are the velocity at time interval t_{t+1} and t_t.

The scatter of velocity and acceleration/deceleration is encoded by a 2D codebook numbered with natural numbers, as shown in Fig. 2. The i^{th} state at time tag t is

denoted as S_t^i, which is defined as a tuple of v_t and a_t whose value satisfy the range defined in i^{th} grid in the codebook. The 2D codebook can be generated by uniformly cut the space into small squares with equal lengths, which is believed to be simple, robust and less sensitive to the length of the sequences used for training the model. Fig. 2 shows an example of the encoding process. However, the velocity sequence is a sequence of continuous values, whereas the entries of state sequence are integers in the codebook.

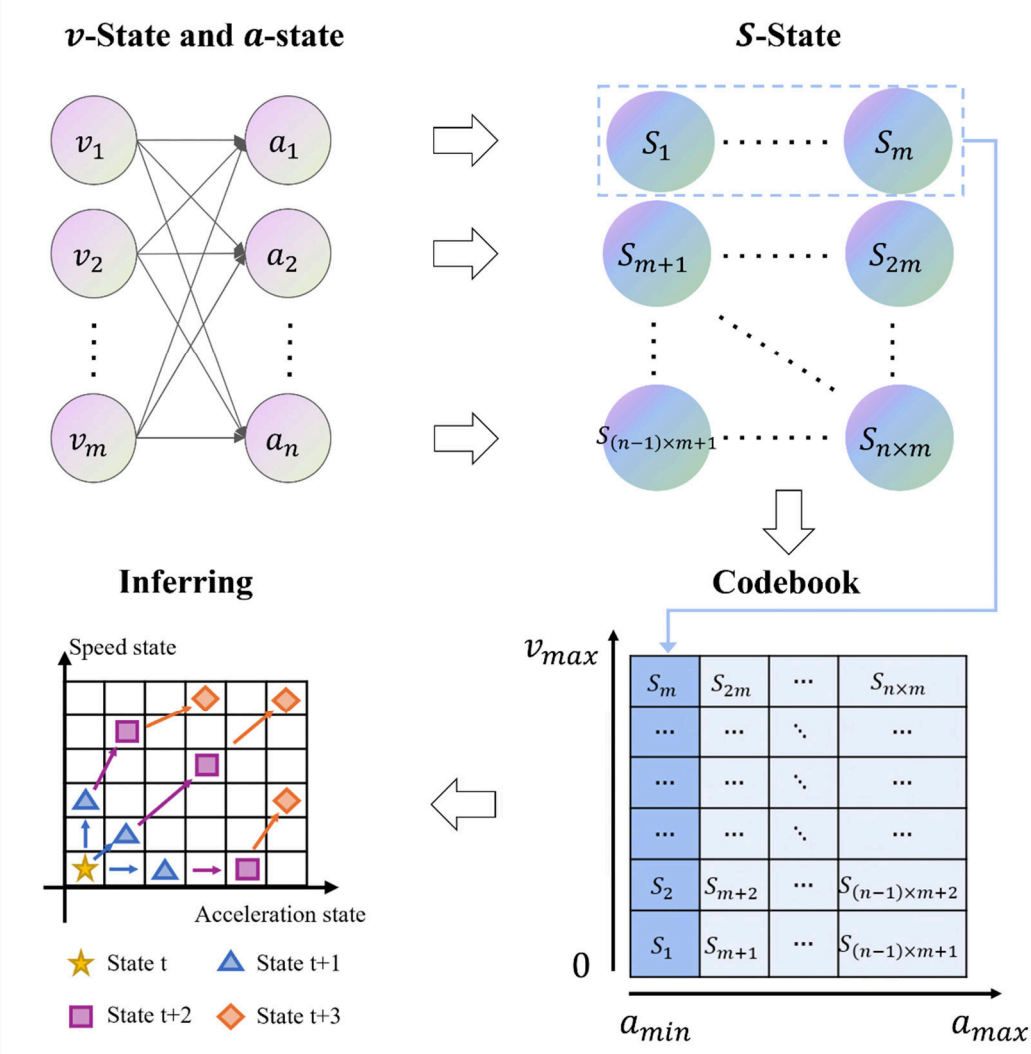


Fig. 2: Illustration of v-state and a-state encoding and inferring using MCMC.

b) Transition probability matrix: The Markov model which gives the relationship

between the current state and the next state is presented in Eq. (5). P_{ij} can be calculated by Eq. (6).

$$P\left(S_{t+1} = S_j \middle| S_t = S_i\right) = P_{ij} \tag{5}$$

$$P_{ij} = \frac{N_{ij}}{\sum_{j=1}^{n} N_{ij}} \tag{6}$$

where t is an arbitrary time tag; P_{ij} is the transition probability of the random variable transient from the current state S_i to the next state S_j. N_{ij} is the number of transitions from state S_i to state S_j; n is the total state number.

The transition probability matrix TPM constituted by the transition probability P_{ij} is shown in Eq. (7).

$$TPM = \begin{pmatrix} P_{11} & P_{12} & \cdots & P_{1n} \\ P_{21} & P_{22} & \cdots & P_{2n} \\ \cdots & \cdots & \cdots & \cdots \\ P_{m1} & P_{m2} & \cdots & P_{mn} \end{pmatrix} \tag{7}$$

where P_{mn} is the probability of the transition from state S_i to state S_j, and m is equal to n in this case.

c) State inferring: Considering the large size of 2D state transition matrix, a Metropolis-Hastings based Markov Chain sampler is designed for state inferring, replacing the conventional multiplication of the large TPM [24]. Specifically, the core idea is to start from state S_t at time t and the transition to state S_{t+1} is accepted or rejected based on the Hastings ratio $\alpha(S_t, S_{t+1})$ [25]. To elaborate, a candidate state S_{t+1} is first randomly generated from the proposal normal distribution $q(S_t|S_{t+1})$. With the selected candidate state S_{t+1}, the transition probability $p(S_{t+1})$ from state S_t to S_{t+1} is obtained from the TPM presented in Eq. (7). Following the similar process for the calculation of $q(S_{t+1}|S_t)$ and $p(S_t)$ for the transition from state S_{t+1}

to S_t, the Hastings ratio $\alpha(S_t, S_{t+1})$ is determined in Eq. (8). The state S_{t+1} is accepted if a random value between 0 and 1 is less than or equal to $\alpha(S_t, S_{t+1})$, otherwise the state remains S_t at time $t+1$.

$$\alpha(S_t, S_{t+1}) = min\left\{1, \frac{p(S_{t+1})q(S_t|S_{t+1})}{p(S_t)q(S_{t+1}|S_t)}\right\} \tag{8}$$

where $p(S_t)$ and $p(S_{t+1})$ are the invariant distribution obtained from the TPM in Eq. (7); $q(S_{t+1}|S_t)$ and $q(S_t|S_{t+1})$ are the proposal normal distribution.

The M-H sampler infers the next state S_{t+1} at time $t+1$ based on the current state S_t at time t. Similarly, it can infer the state S_{t+2} at time $t+2$, …, the state S_{t+k} at time $t+k$ until the maximum length of the driving cycle. An exemplary demonstration of state inferring is depicted in Fig. 2. Each path in Fig. 2 represents a single instance of sampling from the transition probability distribution, achieved through iterative application of an MCMC sampler. Once the predetermined time duration is reached, sampling stops. Eventually, a sequence of state distribution is obtained at each time.

d) V-A state sequence decoding: After acquiring the state distribution results at each time point, decoding this sequence of states enables the derivation of a comprehensive velocity spectrum and acceleration/deceleration spectrum, by which we can construct a driving cycle.

Step 4 Consistency evaluation: In order to evaluate the consistency of driving cycle constructed by a proposed method, Pearson correlation coefficient (Pearson) and mean absolute percentage error (MAPE) are employed to evaluate consistency of the candidate and the real-world driving cycles [26].

$$Pearson = \frac{\sum_{i=1}^{n}(X_i-\bar{X})(Y_i-\bar{Y})}{\sqrt{\sum_{i=1}^{n}(X_i-\bar{X})^2}\sqrt{\sum_{i=1}^{n}(Y_i-\bar{Y})^2}} \quad (9)$$

$$MAPE = \frac{1}{n}\sum_{i=1}^{n}\left|\frac{X_i-Y_i}{Y_i}\right| \times 100\% \quad (10)$$

where X_i is the value of characteristic assessment parameters of generating driving cycles whose mean value is $\bar{X}$; Y_i is the value of characteristic assessment parameters of real driving cycles whose mean value is $\bar{Y}$.

2.3 Real-world FCEBs data and test setup

This section presents the pre-processing of the running data from the ten FCEBs, which serves as input for the proposed algorithm to generate the typical driving cycle. Additionally, it outlines the experimental setup for the bench test to evaluate the economic performance based on the constructed driving cycle. Section 2.3.1 describes and analyses the real-world data of the ten FCEBs, while Section 2.3.2 provides details on the hardware-in-the-loop (HiL) and the environmental chamber bench test.

2.3.1 Real-world raw data description

As mentioned in Section 2.1, ten PEMFC electric buses are currently operating in Minhang District, Shanghai, China, at approximately 121.41°E, 31.07°N. All ten 18-ton buses are equipped with the same PEMFC system illustrated in Appendix 1, with a rated stack power output of 90 kW. A weekly dataset from these ten vehicles, consisting of approximately 3,797,794 data points, has been selected. These data points are transmitted to the host server and sampled every second. As depicted in Appendix 4 (a), the eleven speed characteristics are shown in a radar chart, compared to the characteristics of the China heavy-duty commercial vehicle test cycle-Bus (CHTC-B)

driving cycle, which is commonly used for buses in China. Appendix 4 (b) provides part of the driving cycle from one FCEB, including both working and refuelling segments. Detailed data for these segments are presented in Table 3. It is evident that the driving patterns of the studied FCEBs differ significantly from those of the CHTC-B driving cycle. This disparity could potentially result in inaccurate economic assessments and mislead strategy improvement efforts. The speed range and acceleration/deceleration range are divided into 61 and 10 states respectively. Specifically, the speed value at 0 km/h is classified as a separate state considering the frequent start-stop driving patterns of FCEBs.

Table 3: Eleven speed characteristics of the CHTC-B, the real-world working segments and the real-world refuelling segments.

No.	Characteristics	Unit	CHTC-B	Real-world working segment	Real-world refuelling segment
1	Maximum speed	km/h	45.60	49.84	60.33
2	Maximum acceleration	m/s^2	1.26	3.91	5.34
3	Minimum deceleration	m/s^2	-1.32	-5.21	-4.50
4	Average speed	km/h	15.08	15.53	28.05
5	Average running speed	km/h	19.43	23.02	33.90
6	Average acceleration (>0)	m/s^2	0.48	0.54	0.50
7	Average deceleration (<0)	m/s^2	-0.54	-0.57	-0.55
8	Ratio of acceleration	%	29.16	27.71	31.86
9	Ratio of deceleration	%	25.88	26.06	29.57
10	Ratio of cruising	%	22.60	14.57	21.71
11	Ratio of idling	%	22.37	31.66	16.86

2.3.2 Test setup: hard-ware-in-the-Loop (HiL) and environmental chamber bench test

As shown in Fig. 3, a comprehensive and precise solution is presented to evaluate the economic performance of a fuel cell system, specifically focusing on the hydrogen

consumption per 100 kilometres under the constructed typical driving cycles obtained by the novel method described in Section 2.2. The experiment consists of two core components: hardware-in-the-Loop (HiL) testing and the environmental chamber bench testing.

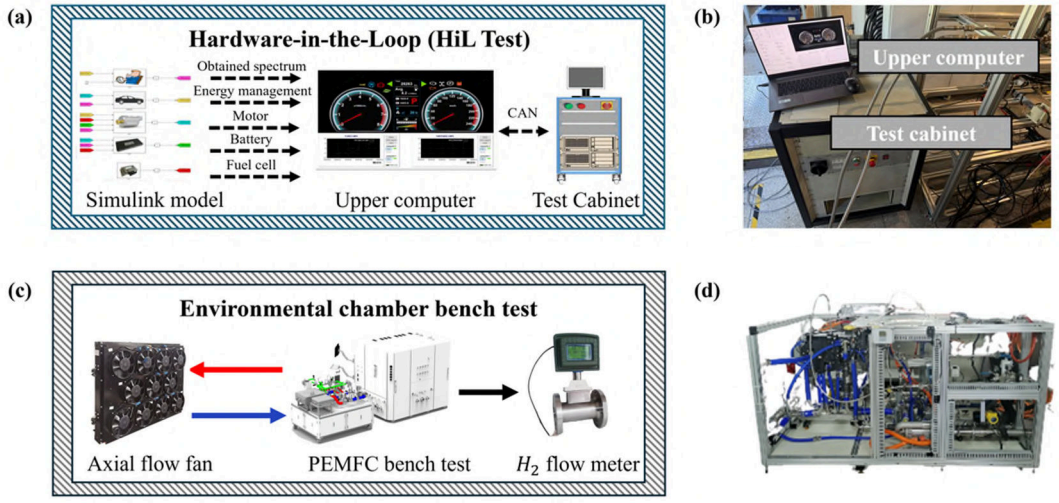


Fig. 3: Illustration of the HiL and bench test: (a) Sketch map of the HiL test setup; (b) Photo of the HiL test; (c) Sketch map of the environmental chamber bench test; (d) Photo of the environmental chamber bench test.

As illustrated in Fig. 3 (a) and (b), the hardware-in-the-loop (HiL) test setup aims to simulate the system performance in real-world conditions, providing crucial data for economic evaluation. An upper computer with the Simulink model manages the energy spectrum including the Lithium-ion battery and the PEMFC system operation. The test cabinet integrated with the fuel cell system is equipped with a hydrogen flow meter to accurately measure hydrogen consumption.

As the primary novelty of this paper is the economic assessment based on the typical driving cycles, the details of the Simulink modelling are provided in [27]. The simulation experiment was conducted with the primary objective of achieving a State

of Charge (SOC) balance at the beginning and end of the test. The experiment was designed to evaluate the performance of the PEMFC system under specified driving cycles, and the resulting fuel cell system power spectra are obtained based on energy management.

Throughout the simulation, the vehicle was maintained in a fully powered state to ensure consistent and reliable data collection. The energy management strategy employed a stabilization period of 30 seconds, allowing for stable system conditions before data recording commenced.

The PEMFC system start-stop strategy was configured to adhere to real-world vehicle settings. Specifically, the PEMFC system was programmed to activate only when the SOC fell below 40%. Consequently, any instances where the PEMFC system remained inactive during the initial stages of the simulation were indicative of SOC levels exceeding 40%. This strategy allowed for a comprehensive analysis of the PEMFC system behaviour and its impact on overall system performance, particularly in scenarios where SOC management is crucial for optimal operation.

On the other hand, as shown in Fig. 3 (c) and (d), the environmental chamber bench test creates a controlled environment for comprehensively assessing the fuel cell system's performance. This area features a PEMFC benchmark testing system and an axial flow fan used to simulate the vehicle's heat dissipation capabilities, ensuring test conditions closely resemble practical application scenarios. Similarly, a hydrogen flow meter is also utilized in this area to precisely record hydrogen consumption, further validating the system's economic performance.

3 Results and discussions

This section analyses the details of the verification and validation results based on the real-time FCEBs running data detailed in Section 2.3. Section 3.1 offers the application combining AGNES from velocity characteristics and GPS signals. Section 3.2 verifies and validates the proposed 2D MCMC algorithm for the two types of FCEBs using the two experimental bench tests detailed in Section 2.3. Section 3.3 provides three sets of comparative analysis, focusing on adaptiveness, accuracy, and computational costs of the proposed new method versus conventional methods.

3.1 Ten FCEBs running data processing

Using the AGNES approach, the eleven dynamic characteristics of the ten FCEBs are categorized into two groups as depicted in Fig. 4. The heat map in Fig. 4 (a) illustrates the normalized relevance of these characteristics across all ten buses. Buses No. 4, 6, and 7 exhibit relatively higher average running speeds, higher average acceleration/deceleration, and lower cruising and idling ratios. This indicates that the driving patterns of type 1 (buses No. 4, 6, and 7) are more intense compared to the other seven buses of type 2. As shown by the ten radar charts in Fig. 4 (b) and (c), type 1 and type 2 display distinct shapes. Furthermore, considering GPS signals, the three buses of type 1 follow route 2, while the seven buses of type 2 follow route 1, as depicted in Appendix 3.

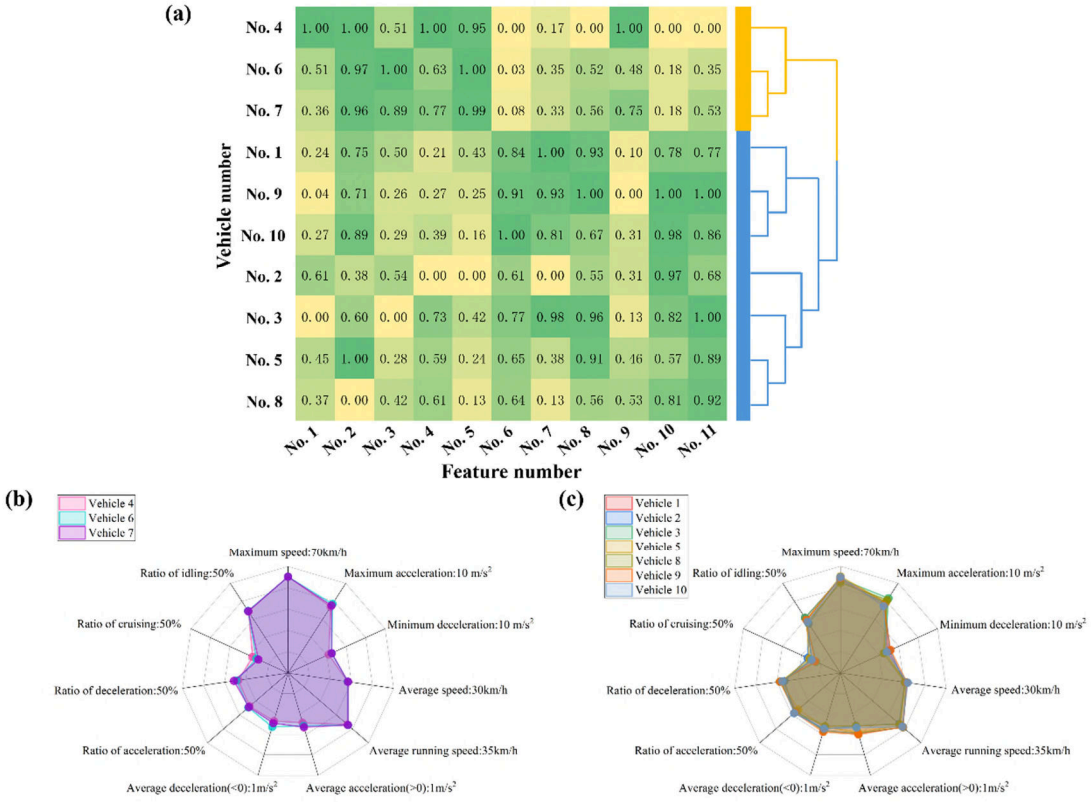


Fig. 4: Hierarchical clustering diagram based on AGNES, incorporating two types of radar charts representing eleven speed characteristics: (a) Heat map of the normalised relevance of eleven speed characteristics of ten FCEBs using AGNES; (b) Radar chart of the eleven characteristics of Type 1 FCEBs, clustered as yellow lines in Fig. 4 (a); (c) Radar chart of the eleven characteristics of Type 2 FCEBs, clustered as blue lines in Fig. 4 (a).

3.2 Verification and validation results and analysis on two bench tests

Based on the clustering outcomes detailed in Section 3.1, Fig. 5 presents the velocity-acceleration/deceleration encoding codebook for two distinct bus types, comprising 2,632,973 data points for Type 1 buses and 1,164,821 data points for Type 2 buses. Specifically, Fig. 5 (a) and (b) exhibit the scatter plots for the working and refuelling intervals, respectively, of Type 1 buses. Conversely, Fig. 5 (c) and 11(d) depict the corresponding data for Type 2 buses. By dividing the velocity and power

ranges into 61 and 10 intervals respectively, the aggregate number of state encoding is 610. The colour gradient from blue to yellow in the scatter points signifies the varying number of state encodings, as exemplified in Fig. 2 of Section 2.2.

A notable observation from the acceleration/deceleration and speed ranges of the working segments in Fig. 5 (a) and (c) is that Type 1 buses attain a maximum speed approximately 5 km/h higher than Type 2 buses. Furthermore, a comparative analysis of Fig. 5 (a) versus (c) and Fig. 5 (b) versus (d) reveals that the acceleration/deceleration spans a broad range across all speed levels, with a discernible trend of decreasing acceleration/deceleration as speed decreases. This finding underscores the intricate relationship between velocity and acceleration/deceleration in both bus types, offering valuable insights for the following driving cycle generation and accurate economic assessment.

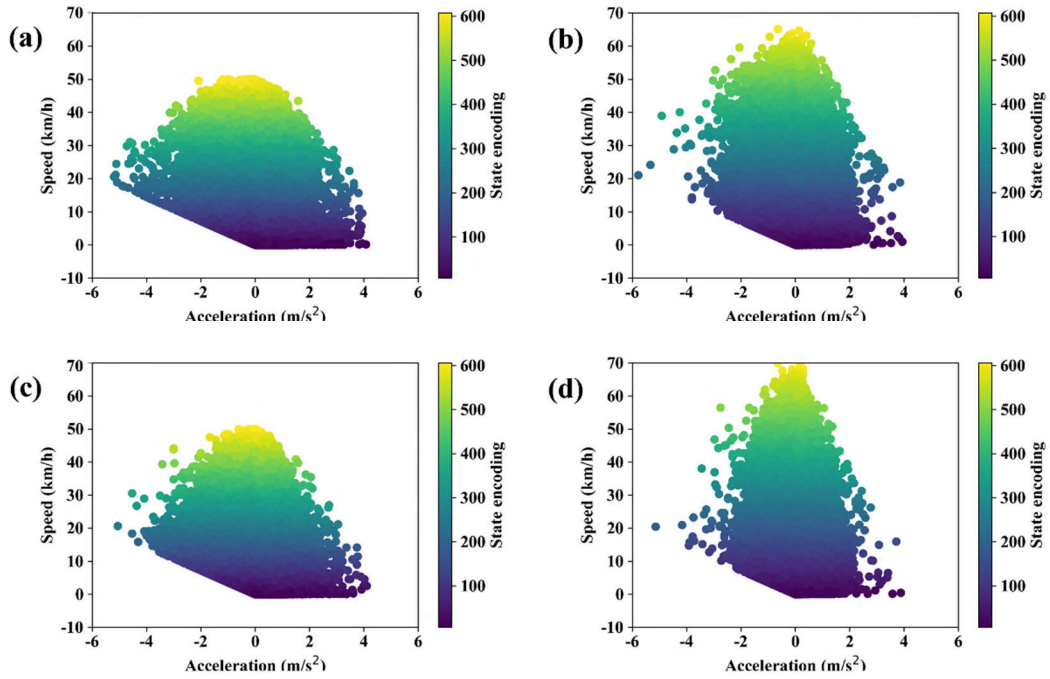


Fig. 5: Velocity-acceleration/deceleration encoding using data from the studied FCEBs: (a) Working segments for Type 1 buses; (b) Refuelling segments for Type 1 buses; (c) Working segments for Type 2 buses; (d) Refuelling segments for Type 2 buses.

Using the velocity-acceleration/deceleration encoding codebook for the two driving segments and bus types shown in Fig. 5, four 610×610 state transition probability matrices are obtained as presented in Fig. 6 and the order of these four figures are the same as Fig. 5. The four smaller figures on the right-hand side of Fig. 6 are 30×30 zoomed-in views of the corresponding 610×610 figures, providing a clearer perspective. The bar charts in Fig. 6 represent the probability of transitioning from one velocity-acceleration/deceleration encoding state at time t to another at time $t+1$. For instance, in Fig. 6 (a) for the working segments of Type 1 buses, the probability of transitioning from encoding state 26 (velocity at 0.83 to 1.66 km/h and acceleration/deceleration at -1.18 to -0.13 m/s^2) at time t to encoding state 7 (velocity at 0 km/h and acceleration/deceleration at -0.13 to 0.93 m/s^2) is 0.80, and to encoding state 17 (velocity at 0 to 0.83 km/h and acceleration/deceleration at -0.13 to 0.93 m/s^2) is 0.14. Consequently, during the generation of driving cycles for the working segments of Type 1 buses, if the velocity is between 0.83 to 1.66 km/h and the acceleration/deceleration is between -1.18 to -0.13 m/s^2 at time t, indicating a decreasing trend, and at time $t+1$ the velocity is predicted to be 80% likely at 0 km/h and 14% likely at 0 to 0.83 km/h. Accordingly, this indicates that out of 527 total transition data points from time t at encoding state 26 to time $t+1$, 420 data points transitioned to encoding state 7, and 72 data points transitioned to encoding state 17.

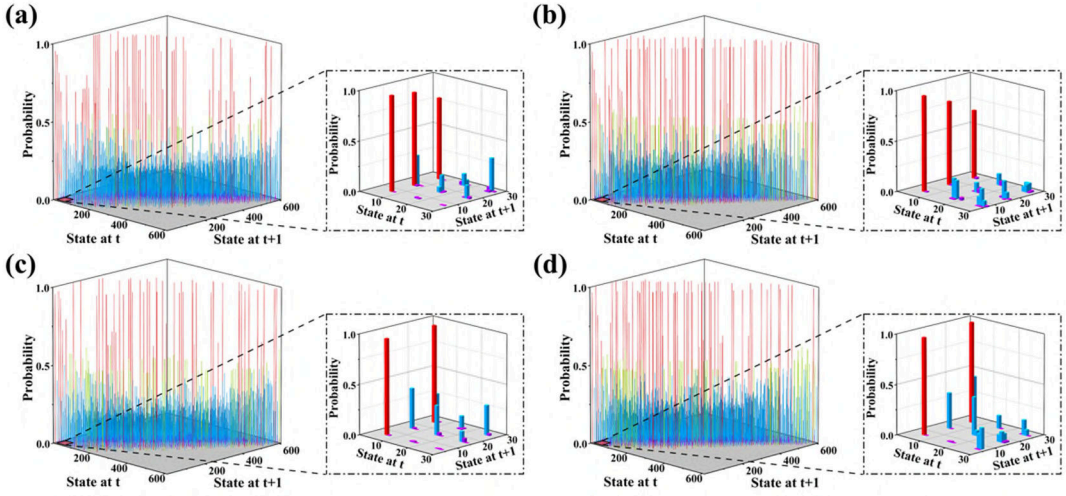


Fig. 6: Four 610×610 state transition probability matrixes established based on the codebooks illustrated in Fig. 5: (a) Working segments for Type 1 buses; (b) Refuelling segments for Type 1 buses; (c) Working segments for Type 2 buses; (d) Refuelling segments for Type 2 buses..

The velocity and acceleration/deceleration spectrums of the four constructed driving cycles including working and driving segments for Type 1 and 2 FCEBs are illustrated in Fig. 7. It is obvious that for both Type 1 and 2 FCEBs, the maximum speed values of working segments are much smaller than the values of refuelling segments but the acceleration/deceleration variations of working segments are more intensive.

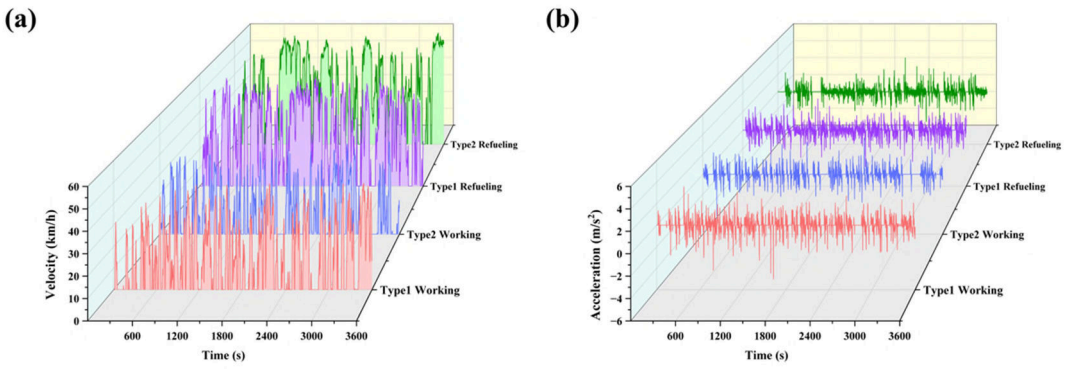


Fig. 7: Velocity and acceleration/deceleration spectrums of the four constructed driving cycles including working and refuelling segments for Type 1 and 2 buses: (a) Velocity spectrums; (b) Acceleration/Deceleration spectrums.

The velocity and power spectrums of four driving cycles of Type 1 buses are presented in Fig. 8. Specifically, Fig. 8 (a) and (c) display the velocity spectrums in red, selected from real-world working and refuelling segments. These segments exhibit speed characteristics that are consistent with the weekly average values. The grey curves in Fig. 8 (a) and (c) represent the corresponding power spectrums, obtained using the same energy management strategy as the studied real-world FCEBs, as detailed in Section 2.3. Fig. 8 (b) and (d) present the constructed velocity and power spectrums in blue and green, respectively. The velocity spectrums are generated by using the transition probability matrixes as shown in Fig. 6. Notably, the characteristics of the velocity and power spectrums under the same driving segments appear similar, indicating that the proposed algorithm effectively captures the essential dynamics of the buses' behaviour and can be reliably used for further analysis and optimization of the driving cycles. The velocity and power spectrums for Type 2 buses are presented in Appendix 5. The detailed economic assessment of the eight driving cycles are compared in Table 4.

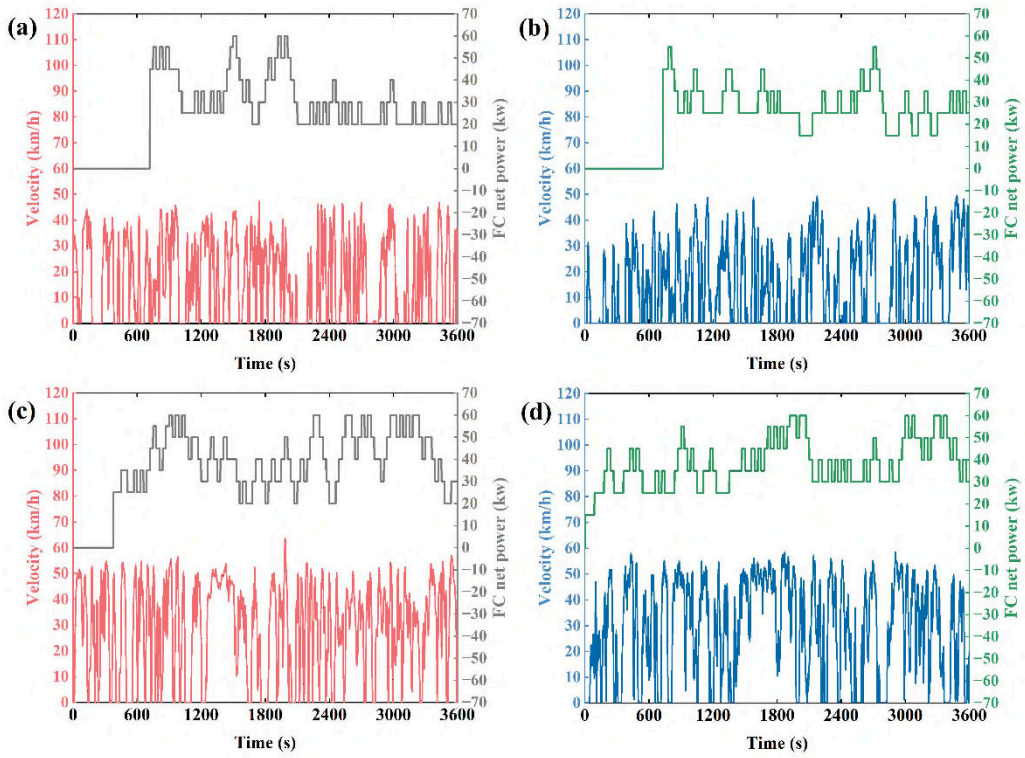


Fig. 8: Velocity and power spectrum across real-world and constructed driving cycles by the proposed method for Type 1 buses: (a) Real-world working segments; (b) Constructed working segments; (c) Real-world refuelling segments; (d) Constructed refuelling segments.

In Table 4, the economic assessment of hydrogen consumption for two types of FCEBs is presented in this section. The analysis compares the real-world driving cycles with the constructed typical driving cycles using the innovative method proposed in this paper. The focus is on the hydrogen consumption per 100 kilometres ($kg/100\ km$) for both working and refuelling segments, as evaluated through Hardware-in-the-Loop (HiL) and bench tests. For data security of the studied FCEBs, the parameters of the tests are set more conservatively than the ones of the real-world buses, resulting in a higher hydrogen consumption value than the real-world buses. Therefore, for the

consistency and comparability of the proposed approach, the vehicle parameters are kept the same for both the HiL and bench tests.

Table 4: Economic assessment of real-world and constructed driving cycles, including working and refuelling segments for Type 1 and 2 buses, based on HiL test and bench test results.

Bus type	Driving cycle type	Segment type	Unit	Economic assessment (H_2 consumption per 100 km)	
				HiL test result	Bench test result
Type 1	Working	Real-world	$kg/100\,km$	8.29	8.57
Type 1	Working	Constructed	$kg/100\,km$	8.39	8.79
Relative error between these two cycles			/	1.21%	2.57%
Type 1	Refuelling	Real-world	$kg/100\,km$	7.30	7.92
Type 1	Refuelling	Constructed	$kg/100\,km$	7.52	8.07
Relative error between these two cycles			/	3.01%	1.90%
Type 2	Working	Real-world	$kg/100\,km$	9.07	9.67
Type 2	Working	Constructed	$kg/100\,km$	9.18	9.83
Relative error between these two cycles			/	1.20%	1.65%
Type 2	Refuelling	Real-world	$kg/100\,km$	7.09	7.42
Type 2	Refuelling	Constructed	$kg/100\,km$	7.25	7.54
Relative error between these two cycles			/	2.23%	1.62%

For Type 1 FCEBs in the working segment, the real-world economic assessment showed an average hydrogen consumption of 8.29 $kg/100\,km$ in the HiL test and 8.57 $kg/100\,km$ in the bench test. The constructed driving cycles, on the other hand, yielded 8.39 $kg/100\,km$ and 8.79 $kg/100\,km$ respectively. The relative error between the real-world and constructed conditions was a minimal 1.21% for the HiL test and 2.57% for the bench test, indicating a close alignment between the two. Besides, for the refuelling segment of Type 1 FCEBs, the hydrogen consumption of the real-world conditions based on the HiL and bench tests are 7.30 $kg/100\,km$ and 7.92 $kg/100\,km$ respectively. In comparison, the economic results of the constructed driving cycles are 7.52 $kg/100\,km$ and 8.07 $kg/100\,km$. The relative error was

3.01% for the HiL test and 1.90% for the bench test, further confirming the method's accuracy. Similarly, for Type 2 FCEBs, the relative errors of the constructed driving cycles are 2.23% for the HiL test and a 1.62% for the bench test, further validating the high robustness of the proposed method.

In summary, for both Type 1 and 2 FCEBs, the working segments entail higher hydrogen consumption values compared with the refuelling segments, mainly caused by the lower PEMFC system efficiency at more frequent load variations. It suggests the significance of the acceleration/deceleration on the economic performance of FCEBs. Despite the differences in speed and acceleration/deceleration variations, the eight relative errors for both working and segments of two types FCEBs are between 1.20% and 3.01%, verifying and validating the accuracy and robustness of the proposed real-world data-driven method in constructing driving cycles for FCEBs economic assessment.

3.3 Comparative analysis

This section presents three comparative analyses to manifest the advantages of the proposed 2D MCMC approach. Section 3.3.1 highlights the adaptiveness of the proposed algorithm by comparing it with the CHTC-B and the conventional micro-trips approach. Section 3.3.2 demonstrates the advancements of the proposed 2D MC algorithm in terms of speed and acceleration/deceleration characteristics, contrasting it with the conventional 1D velocity Markov Chain approach. Lastly, Section 3.3.3 provides a comparative analysis between the 2D MCMC algorithm and the 2D Markov Chain algorithm without the Monte Carlo approach, illustrating the low computational

costs while maintaining high accuracy.

3.3.1 Two-dimensional MCMC versus CHTC-B and conventional micro-trips

The constructed driving cycles exhibit improved similarity and reduced errors in condition constructions, thanks to their ability to reflect randomness in actual roads. For instance, when compared to representative driving condition construction methods based on CHTC-B and micro-trip samples as illustrated in Fig. 9, the proposed method eliminates the need for sorting and screening of class samples, thereby avoiding constraints imposed by micro-trip durations.

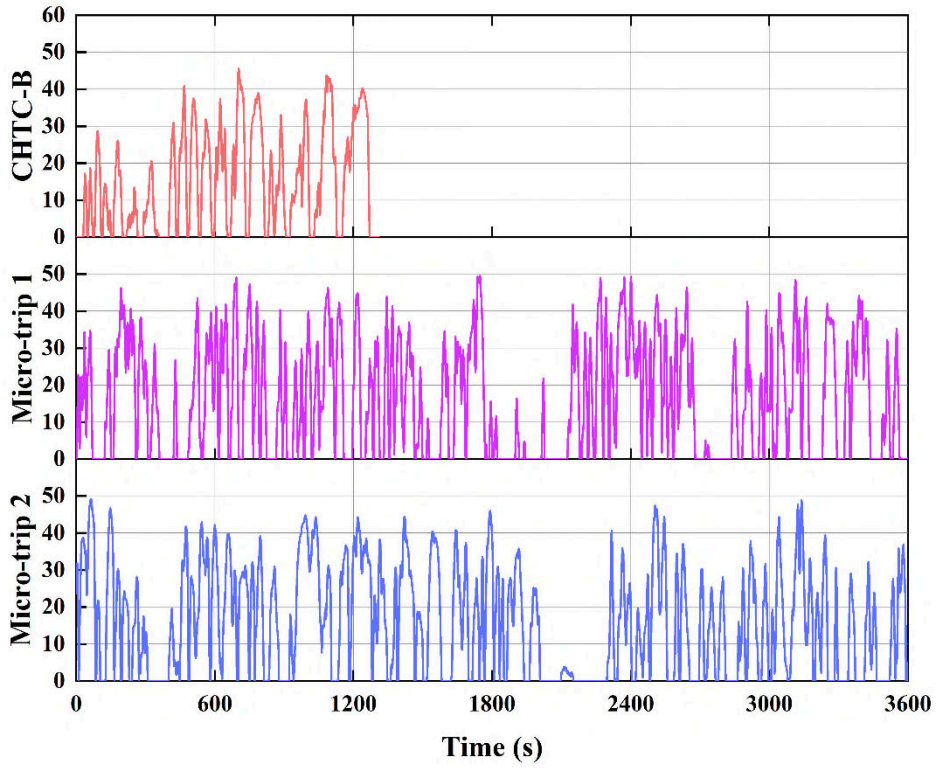


Fig. 9: Velocity spectrums of the CHTC-B, micro-trip 1 and micro-trip 2.

Different from CHTC-B, which reports hydrogen consumption of 6.80 and 6.92 $kg/100\,km$ in HiL and bench tests, real-world working and refuelling segments

consume are 7.09 to 9.07 and 7.42 to 9.67 $kg/100\ km$. The differences of hydrogen consumptions up to 2.27 and 2.75 $kg/100\ km$ (relative errors are 33.38% and 39.74%) under the two segments indicates that the CHTC-B driving cycle cannot be universally applied and may lead to biased estimations of economic performance.

Besides, the hydrogen consumption of the three sets of 1-hour random working segments for Type 1 buses varies significantly from 7.27 to 9.25 $kg/100\ km$. Compared with the value at 8.29 $kg/100\ km$ of the real-world working segment of Type 1 buses listed in Table 4, the relative error ranges from -11.58% to 12.30% which bears a large variation and unsteadiness. It means that the accurate division of original data and correct concatenation of micro-trips are largely dependent on the subjectivity and researchers' experience, which affects the consistency, comparability and efficiency of working condition construction. Furthermore, micro-trip concatenation requires a large amount of specific driving data which is not available for FCEBs at the current stage.

In contrast, the proposed approach considers the global characteristics and the transition probabilities between different driving states with relatively lenient data requirements. It streamlines and enhances the efficiency of the entire driving condition construction process, reducing operational complexity and dependence on human experience. Additionally, this novel approach can be adapted to different needs by adjusting state divisions and transition probability matrices. This flexibility and customizability allow for the construction of driving conditions that align with specific

research objectives and data conditions, making driving condition construction and bench tests highly adaptable.

Table 5: Economic assessment for the CHTC-B and the two driving cycles constructed by conventional micro-trips.

Bus type	Driving cycle type	Segment type	Unit	Economic assessment (H_2 consumption per 100 km)	
				HiL test result	Bench test result
/	CHTC-B	/	$kg/100\ km$	6.80	6.92
Type 1	Micro-trip 1	Working	$kg/100\ km$	9.25	9.36
Type 1	Micro-trip 2	Working	$kg/100\ km$	7.27	7.51

3.3.2 Two-dimensional MCMC versus one-dimensional MC

Driving cycles constructed using the conventional one-dimensional velocity Markov Chain (MC) primarily consider speed transition probability, neglecting the corresponding acceleration transition probability. This conventional approach results in candidate driving cycles with velocities similar to real-world driving cycles but with the notable discrepancy of acceleration values as shown in Fig. 10. The black scatter points in Fig. 10 (a) and (b) represent the velocity and acceleration combinations from 1,000 potential driving cycles derived using both the conventional one-dimensional velocity MC and the proposed two-dimensional velocity-acceleration MCMC. The red points in Fig. 10 (a) and (b) indicate the average speed and acceleration values of a real-world driving cycle segment. Notably, in Fig. 10 (a), all potential scatter points are within the red, yellow, and green contour areas, with none closely matching the real-world values. However, in Fig. 10 (b), the average real-world speed characteristics are situated within the red and yellow contour areas. In more detail, by the comparison over the one-dimensional MC approach, the one-dimensional MC and the 2D MCMC

approach both have similar velocity range under the working segments between 30 and 39 km/h but entails huge differences in acceleration ranges. The red points denoted the ideal points in Fig. 10 (a) and (b) are the average running speed and average acceleration (>0) of the real-world driving cycles of the working segments for Type 1 FCEBs at 33.90 km/h and 0.50 m/s^2. In comparison, when the average running speed is around 33.90 km/h, the average acceleration values of candidate driving cycles range between 0.58 and 0.63 m/s^2 by the one-dimensional MC approach in Fig. 10 (a) and between 0.47 and 0.56 m/s^2 by the proposed 2D MCMC in Fig. 10 (b) respectively. It is obvious that lowest average acceleration value of the driving cycles constructed by the conventional one-dimensional MC approach is much higher than 0.50 m/s^2 of the real-world driving cycles. Through the HiL and bench tests, the lowest relative error observed is 18.3%, much higher than the range within 3.01% by the proposed approach in Table 4. It indicates the paramount importance of acceleration and deceleration on PEMFC system economic performance.

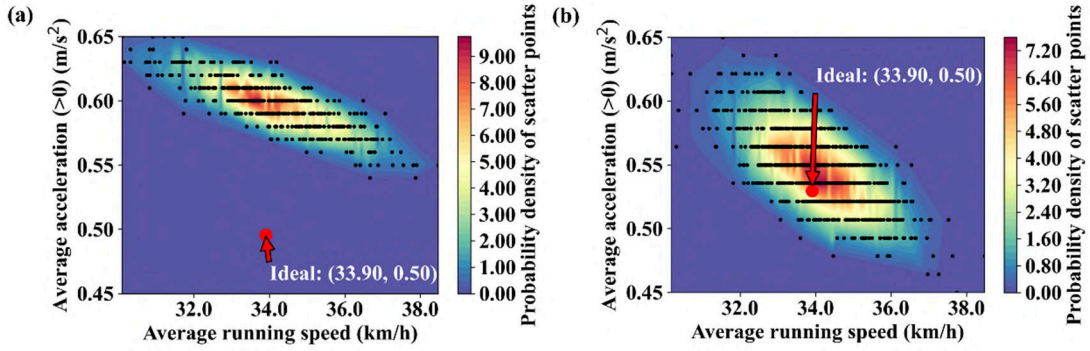


Fig. 10: Contour map of the probability density of 1,000 possible scatter points integrating velocity and acceleration for Type 1 buses refuelling segments based on different approaches: (a) One-dimensional velocity Markov Chain; (b) Two-dimensional velocity-acceleration Metropolis-Hastings based Markov Chain (2D MCMC).

3.3.3 Two-dimensional MCMC versus Two-dimensional MC

Compared to the traditional 60×60 one-dimensional velocity Markov Chain, the proposed 610×610 two-dimensional velocity-acceleration/deceleration model features a significantly larger state transition probability matrix. This enlargement results in significantly higher computational costs due to the multiplication of large matrices, as outlined in Eq. (7). To address this, the 2D MCMC method is employed to sample from the state transition probability matrix using Eq. (8). For the working segments of Type 1 buses, refuelling segments of Type 1 buses, working segments of Type 2 buses, and refuelling segments of Type 2 buses, the numbers of non-zero probabilities in the four state transition probability matrices presented in Fig. 6 are 4,715, 2,845, 4,690, and 3,401, respectively. As depicted in the bar charts in Fig. 11, when compared to the hydrogen consumption per 100 km listed in Table 5 using the 2D MCMC algorithm represented by purple charts, the HiL economic assessment demonstrates similar accuracy with a relative error range of -1.17% to 1.46%. However, the computation time using the 2D MC approach is approximately 1,856 to 1,935 seconds. According to the line chart in Fig. 11, the computation time is reduced by 221 to 244 seconds when using the proposed 2D MCMC for the construction of these four driving cycles, saving up to 12.60% time consumption compared with the 2D MC approach. Therefore, the proposed approach achieves driving cycles with high accuracy, comparable to the MC approach, but with a significantly shorter computation time.

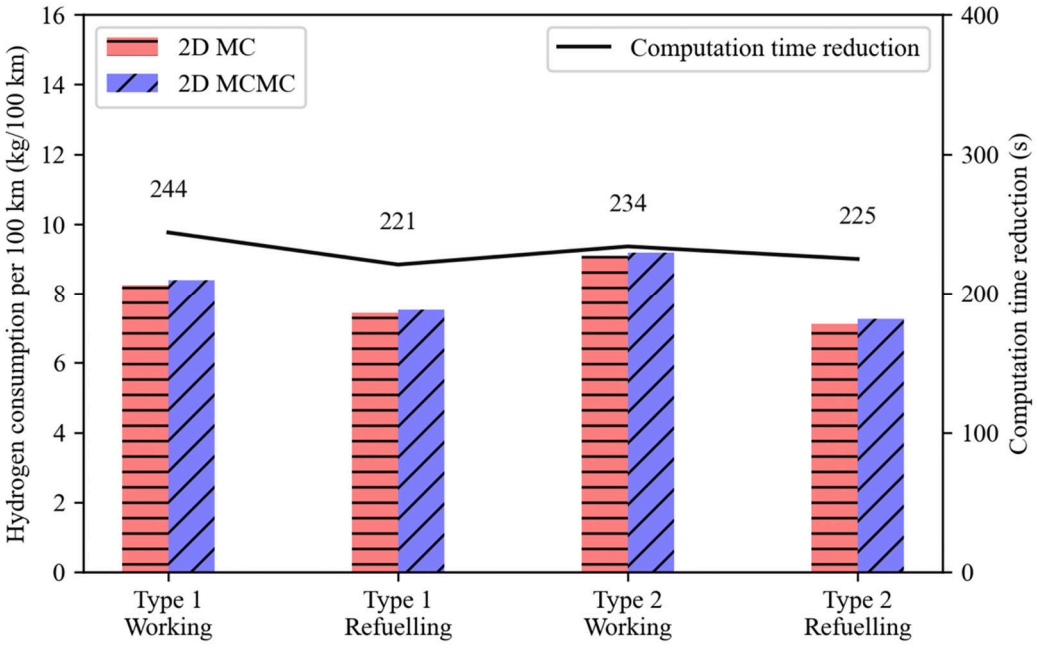


Fig. 11: Comparative results of economic assessment accuracy and computational costs for different approaches.

4 Conclusions

This paper presents a novel hierarchical two-dimensional Markov Chain Monte Carlo (2D MCMC) algorithm, utilizing Metropolis-Hastings (M-H) sampling, to enhance the economic assessment of fuel cell electric buses (FCEBs) through accurately constructed driving cycles. The innovation lies in the new concepts of state encoding and inference, which integrate both speed and acceleration/deceleration considerations while maintaining computational efficiency. This follows the clustering of driving patterns, routes, and hydrogen refuelling station locations using Agglomerative Nesting (AGNES).

The methodology was validated using ten FCEBs operating in Shanghai, China, employing the proposed evaluation system to showcase the algorithm's advancements.

The constructed driving cycles were assessed through a comprehensive system integrating hardware-in-the-loop (HiL) and environmental chamber testing. Compared to real-world driving data, the driving cycles generated by the proposed hierarchical 2D MCMC algorithm showed a relative error in hydrogen consumption of only 1.20% to 3.01%.

To further demonstrate the method's adaptability, accuracy, and efficiency, three sets of comparative analyses were conducted. First, the proposed approach exhibited significantly lower relative errors in hydrogen consumption per 100 km, at only 1.20% to 3.01%, compared to up to 39.74% for the China Heavy-duty Commercial Vehicle Test Cycle for Bus (CHTC-B) and 12.30% for the micro-trip driving cycles. Second, the use of a one-dimensional velocity Markov Chain for estimating acceleration/deceleration resulted in a minimum relative error of 18.3% for the economic assessment of these candidate driving cycles, which is substantially higher than the errors observed with our approach. Lastly, the proposed 2D MCMC algorithm reduced computation time by 12.60% compared to the 2D Markov Chain using matrix multiplication, while maintaining relative errors between -1.17% and 1.46%.

Future work will extend this method to evaluate the economic performance of other PEMFC vehicles, considering factors such as varying loads in PEMFC heavy trucks. Moreover, the precisely constructed driving cycles could serve as inputs for other key technological pathways like energy management strategies, fault diagnosis, and remaining useful lifetime (RUL) estimation.

CRediT authorship contribution statement

Xinjie Yuan: Writing – original draft, Writing – review & editing, Methodology, Conceptualization, Visualization, Funding acquisition. **Miao Xu:** Writing – original draft, Writing – review & editing, Methodology, Software, Visualization. **Zhongjun Hou:** Conceptualization, Supervision, Writing – review & editing. **Wenchuang Chen:** Investigation, Writing – original draft. **Yun Huang:** Conceptualization, Visualization. **Jiaming Lv:** Investigation, Formal analysis, Validation. **Xudong Xu:** Data curation, Formal analysis, Validation. **Luofeng Huang:** Investigation, Writing – review & editing.

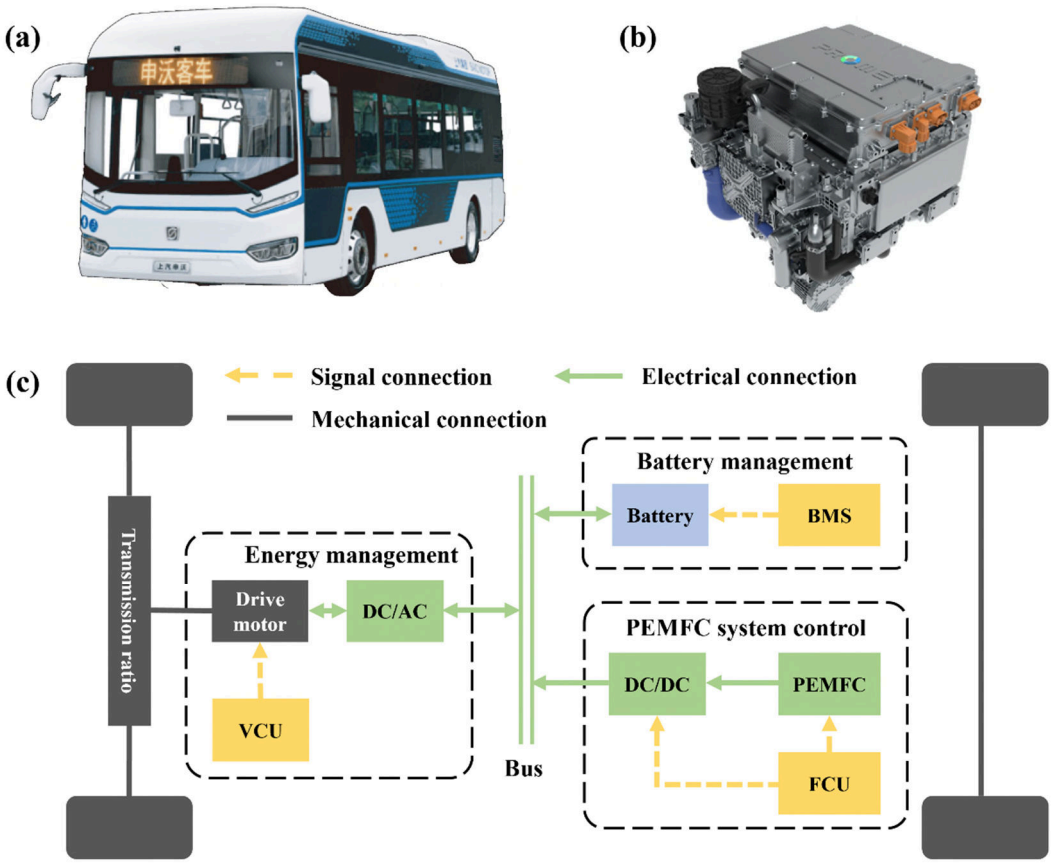
Data Availability

The data that has been used is confidential.

Acknowledgement

This paper is sponsored by Shanghai Pujiang Program (grant No. 23PJ1421700).

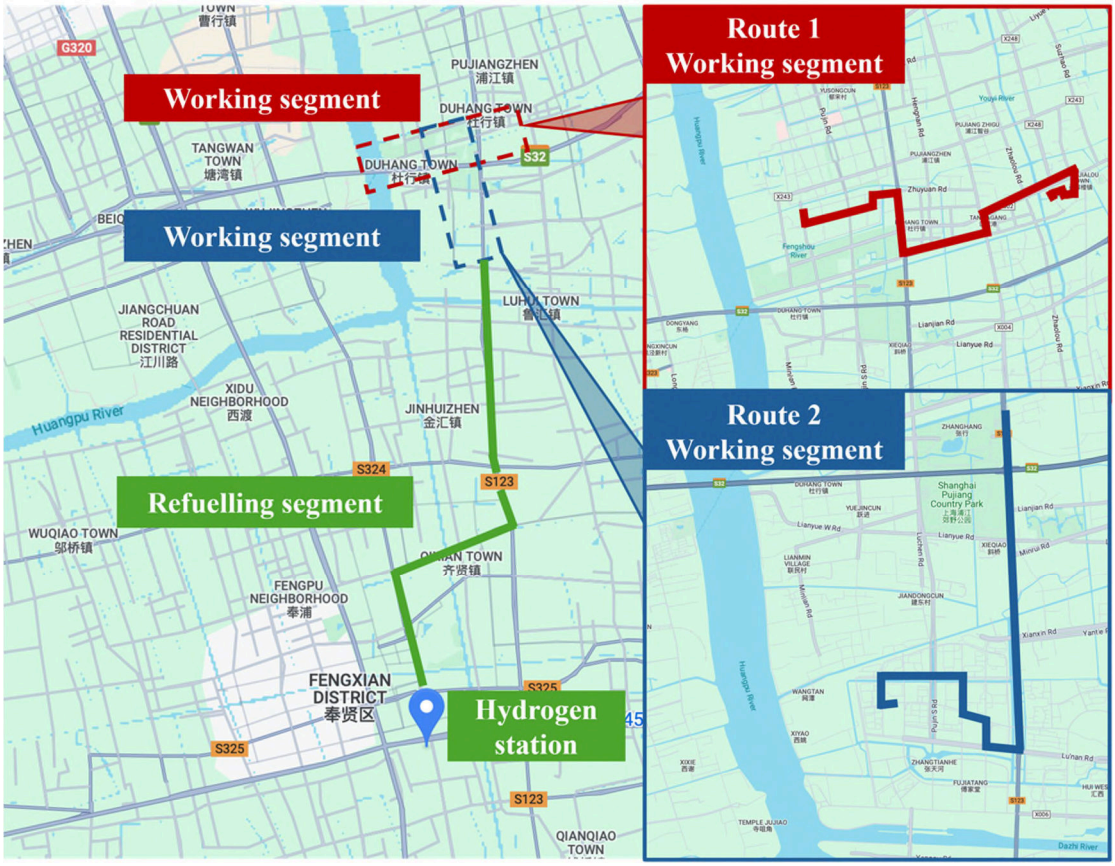
Appendix



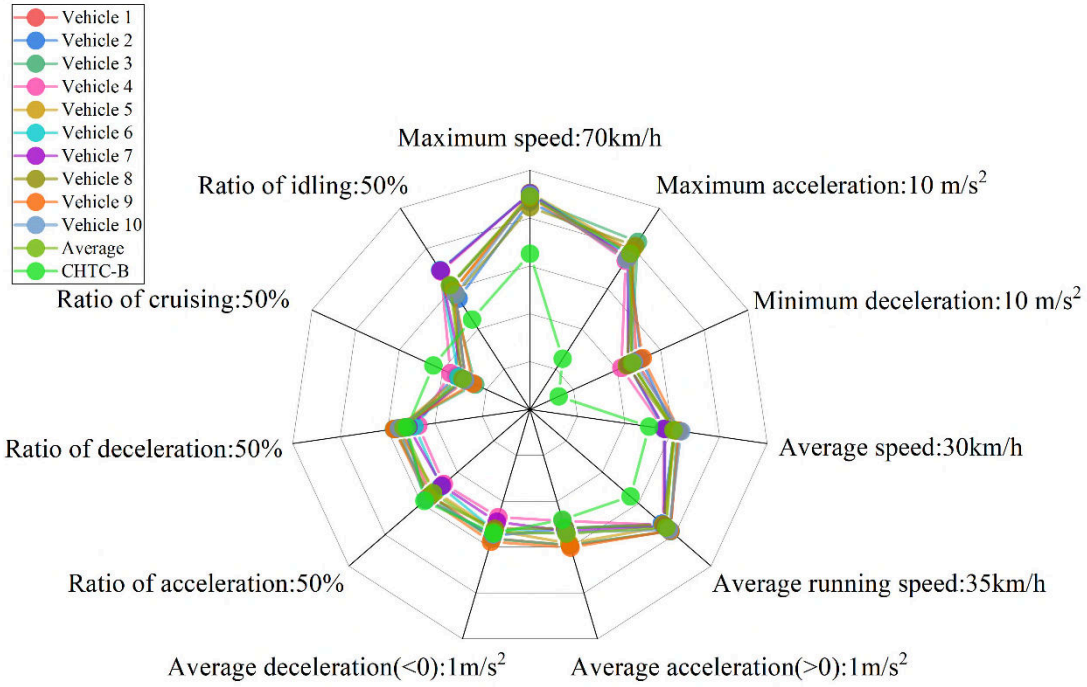
Appendix 1: The studied FCEB running in Shanghai, China: (a) Photo of the FCEB; (b) Photo of the PEMFC system installed on the bus; (c) Schematic diagram of the energy flow.

Appendix 2: Specifications of the PEMFC system installed on the studied Shenwo FCEBs.

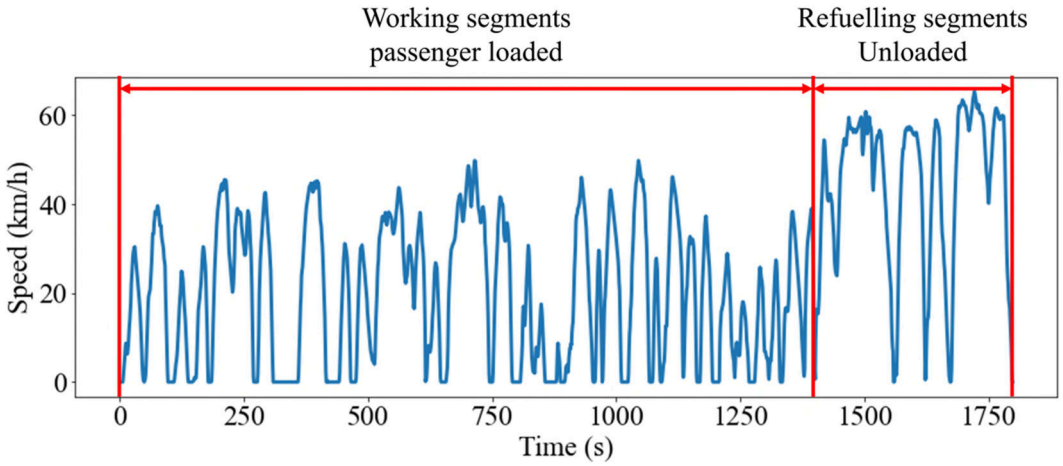
Rated Power (kW)	Maximum Efficiency (%)	Operating temperature (℃)	Size (mm)
90	60	-30 - 95	785 * 660 * 620



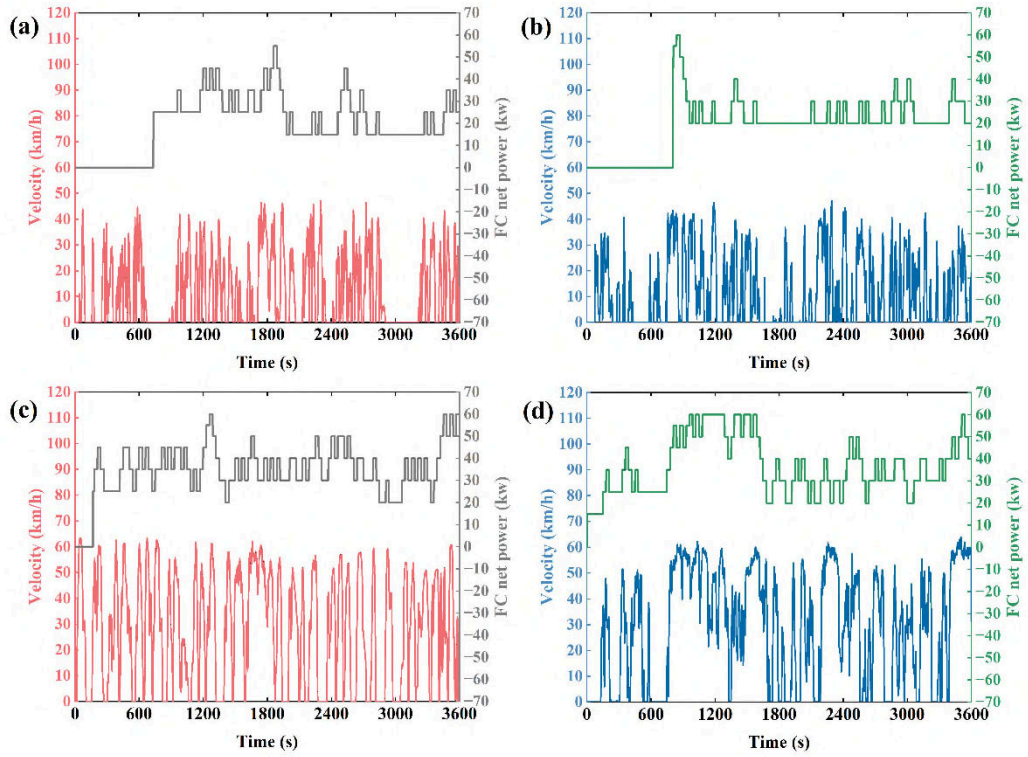
Appendix. 3: Map of the two routes of the studied buses and the nearby hydrogen refuelling station.



Appendix 4: Radar chart of the speed characteristics from ten PEMFC electric buses and the CHTC-B driving cycle.



Appendix 5: Part of the driving cycle from one FCEB, including both working and refuelling segments.



Appendix 6: Velocity and power spectrum across real-world and constructed driving cycles by the proposed method for Type 2 buses: (a) Real-world working segments; (b) Constructed working segments; (c) Real-world refuelling segments; (d) Constructed refuelling segments.

References

[1] M. Singh, M. K. Singla, M. Safaraliev, K. Singh, I. Odinaev, and A. Abdel Menaem, "Advancements and challenges of fuel cell integration in electric vehicles: A comprehensive analysis," *Int. J. Hydrogen Energy*, vol. 88, no. September, pp. 1386–1397, 2024.

[2] L. Iannuzzi, J. A. Hilbert, and E. E. Silva Lora, "Life Cycle Assessment (LCA) for use on renewable sourced hydrogen fuel cell buses vs diesel engines buses in the city of Rosario, Argentina," *Int. J. Hydrogen Energy*, vol. 46, no. 57, pp. 29694–29705, 2021.

[3] H. Togun *et al.*, "A review on recent advances on improving fuel economy and performance of a fuel cell hybrid electric vehicle," *Int. J. Hydrogen Energy*, vol. 89, no. September, pp. 22–47, 2024.

[4] M. A. Aminudin, S. K. Kamarudin, B. H. Lim, E. H. Majilan, M. S. Masdar, and N. Shaari, "An overview: Current progress on hydrogen fuel cell vehicles," *Int. J. Hydrogen Energy*, vol. 48, no. 11, pp. 4371–4388, 2023.

[5] X. Yuan, Y. Liu, and R. Bucknall, "Optimised MOPSO with the grey relationship analysis for the multi-criteria objective energy dispatch of a novel SOFC-solar hybrid CCHP residential system in the UK," *Energy Convers. Manag.*, vol. 243, p. 114406, 2021.

[6] J. Zhang, Z. Wang, P. Liu, Z. Zhang, X. Li, and C. Qu, "Driving cycles construction for electric vehicles considering road environment: A case study in Beijing," *Appl. Energy*, vol. 253, no. 5, p. 113514, 2019.

[7] O. A. Huzayyin, H. Salem, and M. A. Hassan, "A representative urban driving cycle for passenger vehicles to estimate fuel consumption and emission rates under real-world driving conditions," *Urban Clim.*, vol. 36, no. June 2020, p. 100810, 2021.

[8] P. Seers, G. Nachin, and M. Glaus, "Development of two driving cycles for utility vehicles," *Transp. Res. Part D Transp. Environ.*, vol. 41, pp. 377–385, 2015.

[9] Y. Xinjie, Z. Linlin, and H. Zhongjun, "A Novel Real-Time Data-Based PEMFC Performance Evaluation Model Using Improved PCA-KMEANS-XGBOOST for PEMFC Hybrid Vehicles in China," in *Proceedings of China SAE Congress: Selected Papers*, 2023, p. 322.

[10] Z. Chen and R. Xiong, "Driving cycle development for electric vehicle application using principal component analysis and k-means cluster: With the case of Shenyang, China," *Energy Procedia*, vol. 142, pp. 2264–2269, 2017.

[11] X. Yuan, Y. Liu, and R. Bucknall, “A novel design of solid oxide fuel cell-based combined cooling, heat and power residential system in the UK,” in *2019 8th International Conference on Renewable Energy Research and Applications (ICRERA)*, 2019, pp. 212–217.

[12] Z. Wang, J. Zhang, P. Liu, C. Qu, and X. Li, “Driving cycle construction for electric vehicles based on Markov chain and Monte Carlo method: A case study in Beijing,” *Energy Procedia*, vol. 158, pp. 2494–2499, 2019.

[13] X. Jia *et al.*, “Constructing representative driving cycle for heavy duty vehicle based on Markov chain method considering road slope,” *Energy AI*, vol. 6, p. 100115, 2021.

[14] Z. Dou, C. Zhang, D. Li, Z. Ye, and Y. Wang, “Machine learning-based prediction of battery heat generation management in standard driving cycles to avoid thermal runaway and increasing safety,” *Process Saf. Environ. Prot.*, vol. 188, no. June, pp. 1385–1397, 2024.

[15] X. Lin, G. Zhang, and S. Wei, “Velocity prediction using Markov Chain combined with driving pattern recognition and applied to Dual-Motor Electric Vehicle energy consumption evaluation,” *Appl. Soft Comput.*, vol. 101, p. 106998, 2021.

[16] Q. S. Wei, X. Zhang, and B. S. Oh, “The effect of driving cycles and H2 production pathways on the lifecycle analysis of hydrogen fuel cell vehicle: A case study in South Korea,” *Int. J. Hydrogen Energy*, vol. 46, no. 10, pp. 7622–7633, 2021.

[17] J. Fu *et al.*, “Degradation-oriented real-time power control of fuel cell hybrid vehicles under uncertain driving conditions,” *Int. J. Hydrogen Energy*, vol. 48, no. 78, pp. 30556–30569, 2023.

[18] T. Cahalan, S. Rehfeldt, M. Bauer, M. Becker, and H. Klein, “Experimental set-up for analysis of membranes used in external membrane humidification of PEM fuel cells,” *Int. J. Hydrogen Energy*, vol. 41, no. 31, pp. 13666–13677, 2016.

[19] T. Teng, X. Zhang, H. Dong, and Q. Xue, “A comprehensive review of energy management optimization strategies for fuel cell passenger vehicle,” *Int. J. Hydrogen Energy*, vol. 45, no. 39, pp. 20293–20303, 2020.

[20] Y. Xu, F. E. Gbologah, D. Lee, H. Liu, M. O. Rodgers, and R. L. Guensler, “Assessment of alternative fuel and powertrain transit bus options using real-world operations data : Life-cycle fuel and emissions modeling,” *Appl. Energy*, vol. 154, pp. 143–159, 2015.

[21] S. A. of China, “China automobile test cycle—Part 2: heavy-duty commercial vehicles. National Standard GB/T 15089-2001.,” 2019.

[22] R. Xu, S. Member, and D. W. Ii, “Survey of Clustering Algorithms,” vol. 16, no. 3, pp. 645–678, 2005.

[23] A. Gere, “Recommendations for validating hierarchical clustering in consumer sensory projects,” *Curr. Res. Food Sci.*, vol. 6, no. February, p. 100522, 2023.

[24] K. Song, X. Huang, Z. Cai, P. Huang, and F. Li, “Research on energy management strategy of fuel-cell vehicles based on nonlinear model predictive control,” *Int. J. Hydrogen Energy*, vol. 50, pp. 1604–1621, 2024.

[25] A. Bott, T. Janke, and F. Steinke, “Deep learning-enabled MCMC for probabilistic state estimation in district heating grids,” *Appl. Energy*, vol. 336, no. May 2022, p. 120837, 2023.

[26] H. Xu, J. Zhang, C. Cheng, H. Cao, J. Lu, and Z. Zhang, “A novel metric for evaluating hydro-wind-solar energy complementarity,” *Appl. Energy*, vol. 373, no. January, p. 123926, 2024.

[27] H. Zhou, Z. Yu, X. Wu, Z. Fan, X. Yin, and L. Zhou, “Dynamic programming improved online fuzzy power distribution in a demonstration fuel cell hybrid bus,” *Energy*, vol. 284, no. July, p. 128549, 2023.



https://dspace.org/

Enhanced data-driven economic assessment of fuel cell electric buses utilizing an improved Markov chain Monte Carlo approach

Yuan, Xinjie; Xu, Miao; Hou, Zhongjun; Chen, Wenchuang; Huang, Yun ...

2025-02-10
Elsevier
https://doi.org/10.1016/j.ijhydene.2024.10.431
Yuan X, Xu M, Hou Z, et al., (2025) Enhanced data-driven economic assessment of fuel cell electric buses utilizing an improved Markov chain Monte Carlo approach. International Journal of Hydrogen Energy, Volume 102, February 2025, pp. 732-748

Downloaded from a DSpace repository. https://dspace.org/